ELSEVIER

Tectonophysics 236 (1994) 391–408

TECTONOPHYSICS

Composition of the crust beneath the Kenya rift

Walter D. Mooney [a], Nikolas I. Christensen [b]

[a] *U.S. Geological Survey, 345 Middlefield Road, MS 977, Menlo Park, CA 94025, USA*
[b] *Department of Earth and Atmospheric Science, Purdue University, West Lafayette, IN 47907, USA*

Received 1 October 1992; accepted 5 November 1993

Abstract

We infer the composition of the crust beneath and on the flanks of the Kenya rift based on a comparison of the KRISP-90 crustal velocity structure with laboratory measurements of compressional-wave velocities of rock samples from Kenya. The rock samples studied, which are representative of the major lithologies exposed in Kenya, include volcanic tuffs and flows (primarily basalts and phonolites), and felsic to intermediate composition gneisses. This comparison indicates that the upper crust (5–12 km depth) consists primarily of quartzo-feldspathic gneisses and schists similar to rocks exposed on the flanks of the rift, whereas the middle crust (12–22 km depth) consists of more mafic, hornblende-rich metamorphic rocks, probably intruded by mafic rocks beneath the rift axis. The lower crust on the flanks of the rift may consist of mafic granulite facies rocks. Along the rift axis, the lower crust varies in thickness from 9 km in the southern rift to only 2–3 km in the north, and has a seismic velocity substantially higher than the samples investigated in this study. The lower crust of the rift probably consists of a crust/mantle mix of high-grade metamorphic rocks, mafic intrusives, and an igneous mafic residuum accreted to the base of the crust during differentiation of a melt derived from the upper mantle.

1. Introduction

The Kenya Rift has long attracted the attention of earth scientists as one of the most well-developed Cenozoic rifts in terms of its geomorphic expression, recent faulting, and abundant basaltic volcanism. Early geophysical investigations of the Kenya Rift utilized a broad range of methods to investigate deep crustal structure, including seismic refraction profiles, local earthquake and teleseismic delay-time studies, and gravity and geoelectrical measurements (Swain et al., 1994). These early investigations provided the basis for the first generalized lithospheric cross-sections of the rift. By the middle 1980's a need was generally recognized for a detailed seismological investigation of the crust and sub-crustal lithosphere of the rift. Two major field investigations, KRISP-85 (Kenya Rift International Seismic Project 1985) and KRISP-90 were undertaken to meet this need (Prodehl et al., 1994a). In the KRISP-90 study, the more extensive of the two field studies, detailed seismic refraction profiles were recorded in three directions: along the axis of the Kenya rift, across the central rift, and on the east flank. The results have been used to

SSDI 0040-1951(94)00042-8

define the crustal and upper mantle seismic velocity structure beneath and on the flanks of the rift. In this paper we interpret the crustal composition of Kenya based on a comparison of the crustal velocity structure with laboratory seismic velocity measurements made on Kenyan rock samples.

2. Overview of the geology of Kenya

The geology of Kenya may be generalized as consisting of three geologic provinces: (1) Archean metamorphic rocks of the Nyanza craton in western Kenya; (2) late Proterozoic to Cambrian metamorphic and intrusive rocks of the Mozam-

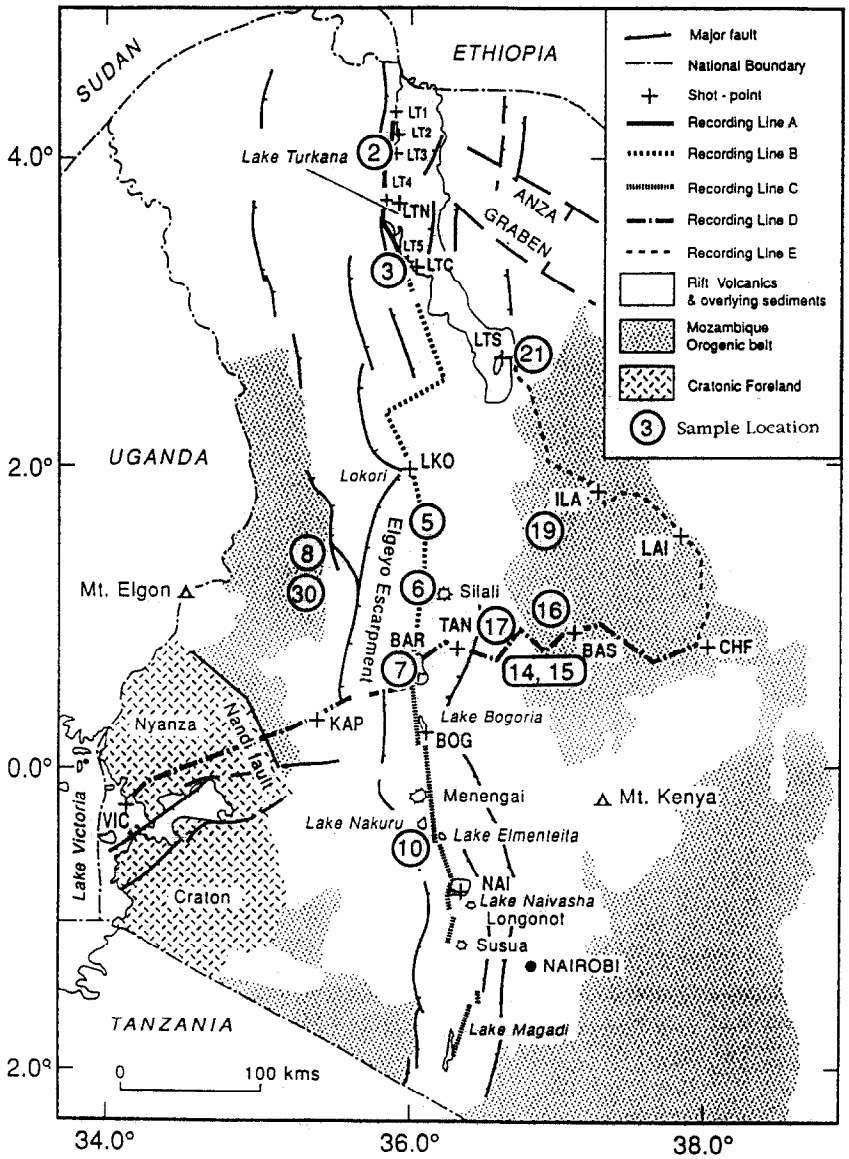

Fig. 1. Location map of the Kenya rift with generalized geology, KRISP-90 seismic refraction profiles, and sample locations for the volcanic and metamorphic rocks whose seismic velocities were determined in this study. Circled numbers refer to sample numbers in Tables 1–3.

bique orogenic belt of central and eastern Kenya; and (3) extensive Cenozoic volcanic rocks associated with rifting that range in age from 35 Ma to recent (Fig. 1). Sedimentary rocks of Cretaceous to Miocene age locally overlie basement rocks, but are not believed to be of significant thickness in the KRISP-90 study area (Morley et al., 1992).

The Archean metamorphic rocks of the Nyanza craton consist of a variety of gneisses cut by intrusive rocks of somewhat younger age. The Mozambique orogenic belt was created during a discontinuous period of faulting, folding and metamorphism that began at approximately 850 Ma (Mosley, 1993). Metamorphism reached greenschist and lower amphibolite grade during this event, and granitoid bodies were emplaced as dikes and sills. The basement rocks of the Nyanza craton and the Mozambique belt were subsequently uplifted and eroded, leaving a virtually planar surface throughout the Mesozoic and early Cenozoic (Baker et al., 1972).

This period of uplift and peneplain development ended in the late Eocene/early Oligocene with the formation of the Kenya rift. The initiation of rifting began with extensive outpourings of olivine-rich basalts, and subsequent eruptions consisting of basaltic, trachytic and phonolitic lavas (Hackman et al., 1990; Smith, 1994; Morley, 1994). These volcanic rocks which now cover the region in a vast mosaic, are estimated to amount to as much as 144,000 km^3 (Williams, 1972). Present-day seismicity and volcanic eruptions within the last few hundred years demonstrate that the Kenya rift is still active.

3. Crustal structure of the Kenya rift and flanking regions

Seismic refraction profiles were recorded (1) along the axis of the rift from northern Lake Turkana to Lake Magadi (in three segments, recording lines A, B, and C; Fig 1), (2) across the rift from Lake Victoria to Chanler's Falls (CHF), and passing through Lake Baringo (BAR; line D), and (3) along the east flank of the rift from Chanler's Falls to southern Lake Turkana (line E, Fig. 1; Prodehl et al., 1994a). The data were recorded at an average station spacing of 1.5 km, with the exception of the northern portion of the axial profile data at Lake Turkana (line A), which had a station spacing of 0.75 km and closely spaced shots in the lake. The crustal velocity models are reported by the KRISP Working Party (1991), and in several papers in this volume. The salient features of the three new crustal velocity models are summarized below. Measurement errors are estimated to be about 10% for depths to major crustal boundaries and 3% for seismic velocities (cf. Mooney, 1989). The consistency of the seismic velocities and depths reported for the three seismic profiles indicates that these error estimates are conservative.

3.1. Axial profile (Fig. 2)

Crustal thickness (i.e., surface, rather than sea level, to Moho) increases from 20 km in the northern Kenya rift beneath Lake Turkana, to 34 km in the southern rift. Supracrustal rocks show a wide range of velocities, varying from 2.0 to 5.2 km/s. The upper crustal basement rocks have seismic velocities of 6.1–6.3 km/s, and are 10–12 km thick in the southern rift and thin to 5–7 km to the north. The middle crust, at a depth of 10–14 km, has an average velocity of 6.5 km/s (6.4 km/s in the north), and thins gradually from 11 km in the south to 8 km in the north (Fig. 2). The lower crust, at a depth of 18–25 km, has an average velocity of 6.8 km/s. This layer is 9 km thick to the south and thins to only 2 km beneath Lake Turkana in the north (Fig. 2). The upper mantle velocity is anomalously low (7.5–7.7 km/s) along the axis of the Kenya rift. Details of the axial crustal structure are provided by Mechie et al. (1994) and Gajewski et al. (1994).

3.2. Cross-profile (Fig. 2)

The crustal thickness determined on the cross-profile varies by 20%. Crustal thickness decreases from 35–40 km on the west flank of the rift to 31 km in the middle of the rift, and increases to 39 km on the east flank. Volcanic rocks (tuffs and flows) are concentrated around the rift axis, and show a wide range of seismic

velocities that are consistent with those determined for the axial profile (Fig. 2). Upper, middle, and lower crustal velocities are 6.1–6.3 km/s, 6.5–6.6 km/s, and 6.7–7.0 km/s, respectively, and are thus consistent with those determined beneath the axial profile. The upper crustal layer thins to 10 km directly beneath the rift, and thickens to as much as 19 km to the west. Crystalline basement rocks are well exposed on the cross-profile outside the rift. Significantly, the anomalously low upper mantle velocity of 7.5–7.7 km/s is restricted to the rift, whereas the velocity reaches 8.1–8.3 km/s on the flanks. Details of this crustal model are provided by Maguire et al. (1994) and Braile et al. (1994).

3.3. East flank profile (Fig. 2)

The upper, middle and lower crustal velocities of 6.0–6.3 km/s, 6.6 km/s, and 6.8 km/s, respectively, determined for the east flank profile are consistent with those reported for the axial and cross-profiles. Crystalline rocks occur at the surface along this profile, with the exception of the northern portion at Lake Turkana. The crust thickens from 27 km beneath southernmost Lake

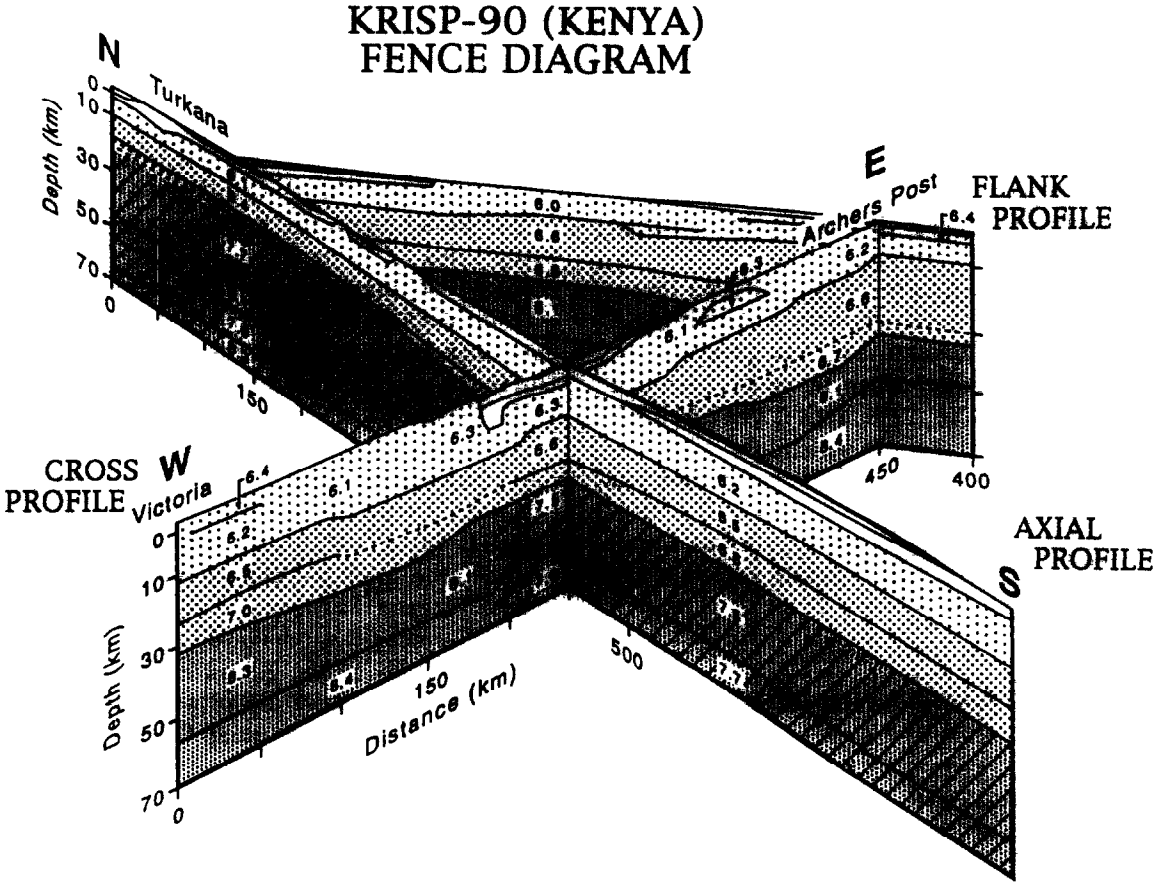

Fig. 2. Fence diagram summarizing the crustal velocity structure of Kenya based on the KRISP-90 investigation (modified from Keller et al., 1994). The axial profile (lines A, B and C, Fig. 1) shows a three-layer crystalline crust with average velocities of 6.2 km/s, 6.5 km/s and 6.8 km/s. The crust thins from south to north, and the upper mantle velocity is 7.5–7.7 km/s. The east–west cross-rift profile (line D, Fig. 1) shows low-velocity volcanics within the rift trough, and crustal velocities that are consistent with the axial profile. The east flank profile (line E, Fig. 1) shows an average crustal thickness of 30 km and three main crustal layers. The seismic velocities in the upper mantle are normal (8.1–8.3 km/s) on the flanks of the rift. The laboratory measurements are compared with average one-dimensional velocity/depth profiles taken from these crustal cross-sections.

Turkana to 35 km in the southeast (Archer's Post, Fig. 2). The upper crust has a nearly uniform thickness of 8–10 km, whereas the middle and lower crust vary in thickness, with the higher-velocity (6.7–6.9 km/s) lower crust attaining a maximum thickness of 12 km in the center of the profile. The upper mantle velocity is 8.1 km/s. Details of this crustal model are provided by Prodehl et al. (1994b).

4. Laboratory studies

Rock samples for laboratory seismic velocity measurements were collected: (1) in the northern rift on the eastern and western shores of Lake Turkana; (2) in the central rift between Lokori (LKO, Fig. 1) and Lake Naivasha; (3) from Proterozoic basement outcrop west of the axial profile; (4) along the portion of the cross-profile between Lake Baringo and Barsalinga (BAS, Fig. 1); and (5) from a basement outcrop west of the middle of the east flank profile (Fig. 1). Where possible, rock samples were collected in close proximity to the seismic profiles. Mineralogies were estimated from petrographic observations (point counts) of thin sections (Table 1) and sample chemistry was determined (Table 2). Classification of the volcanic rocks was based on their chemistry and total alkali–silica diagram of LaBas

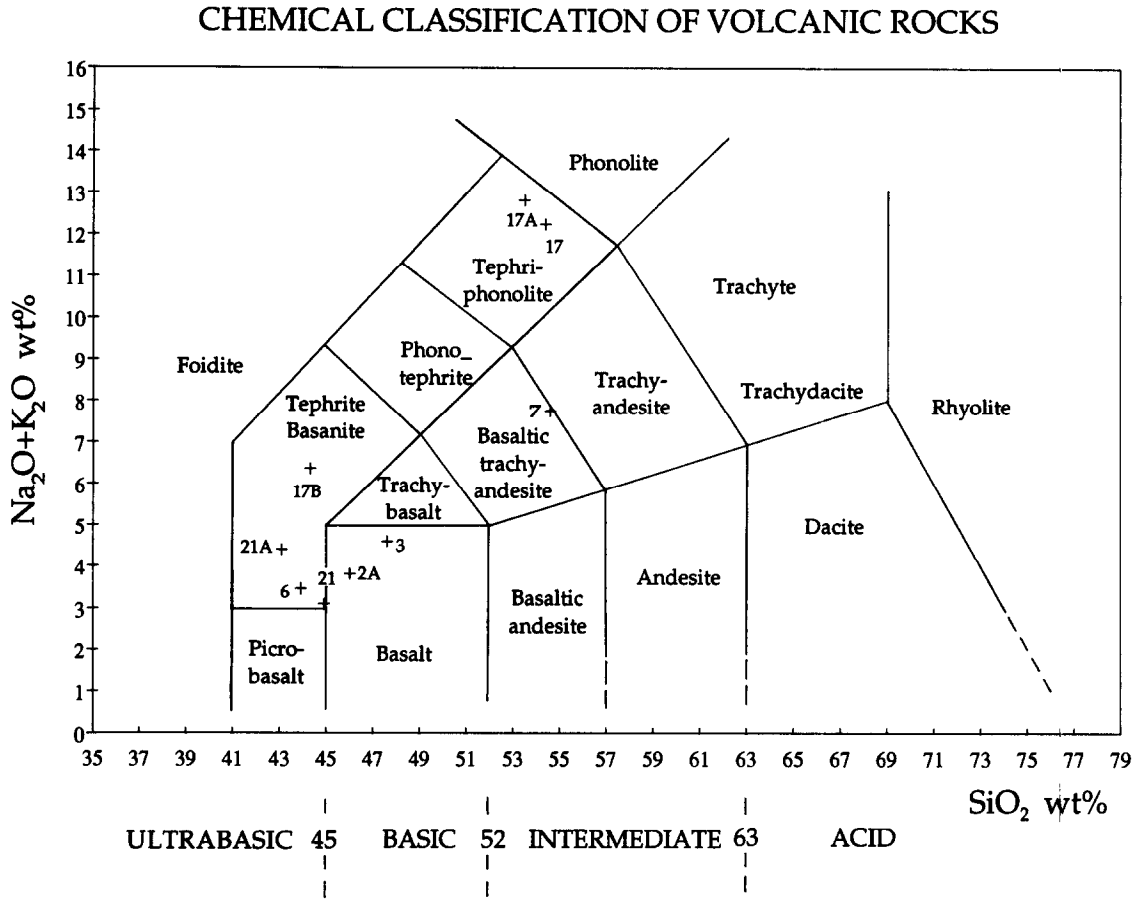

Fig. 3. Classification of volcanic rocks based on silica–alkali abundance (LaBas et al., 1986).

Table 1
Kenya rock samples

Volcanic Rocks

K-2A	Basalt		K-3	Basalt	
	64% plagioclase			55% plagioclase	
	18% pyroxene	groundmass		30% pyroxene	groundmass
	3% magnetite			3% magnetite	
	15% pyroxene	phenocrysts		2% chlorite	
				10% pyroxene	phenocrysts
K-5	Tuff		K-7	Basaltic Trachyandesite	
	15% sanidine	phenocrysts		59% plagioclase	groundmass
	20% vesicles			21% pyroxene	
	65% altered	groundmass		5% magnetite	
				10% plagioclase	phenocrysts
K-6	Tephrite basanite		K-10	Tuff	
	45% plagioclase	groundmass		15% sanidine	phenocrysts
	17% pyroxene	groundmass		20% vesicles	
	6% magnetite			65% altered groundmass	
	2% calcite				
	20% plagioclase	phenocrysts			
	10% pyroxene (altered)	phenocrysts			
K-17	Tephriphonolite		K-17A	Tephriphonolite	
	52% plagioclase			50% plagioclase	
	16% augite			16% augite	
	4% chlorite			4% chlorite	
	30% altered groundmass			30% altered groundmass	
K-21	Tephrite basanite		K-21A	Tephrite basanite	
	50% plagioclase			50% pyroxene	
	26% pyroxene	groundmass		23% plagioclase	groundmass
	4% magnetite			2% magnetite	
	20% pyroxene	phenocrysts		25% plagioclase	phenocrysts

Metamorphic Rocks

K-8	Granitic Gneiss		K-14	Granitic Gneiss	
	60% microcline			58% microcline	
	21% quartz			22% quartz	
	14% plagioclase			17% plagioclase	
	5% biotite			1% garnet	
				1% magnetite	
				1% biotite	
K-15	Granite Gneiss		K-16	Granitic Gneiss	
	64% perthite			52% microcline	
	25% quartz			20% quartz	
	10% plagioclase			17% plagioclase	
	1% biotite			5% biotite	
				5% garnet	
				1% magnetite	
K-19	Dioritic Gneiss		K-30	Tonolite Gneiss	
	40% hornblende			55% palgioclase	
	18% quartz			25% hornblende	
	22% plagioclase			18% quartz	
	10% pumpellyite			1% sphene	
	7% prehnite			1% magnetite	
	2% garnet				
	1% biotite				

Table 2

	K-2a	K-5	K-6	K-7	K-8	K-10	K-14	K-15	K-16	K-17	K-17a	K-17b	K-18	K-19	K-20	K-21	K-21a	K-30	
SiO_2	46.00	65.60	43.90	54.60	66.70	61.80	71.00	65.80	71.60	54.40	53.50	44.30	75.10	50.90	3.50		44.90	43.10	61.00
Al_2O_3	14.10	9.23	14.80	15.70	17.90	15.50	13.80	18.40	13.30	17.70	18.10	14.70	14.80	16.70	0.89		13.80	12.50	14.70
CaO	11.70	0.57	11.00	5.42	1.32	1.00	2.10	1.20	1.96	1.65	1.92	10.50	0.51	9.69	28.90		11.30	10.50	7.12
MgO	8.17	0.14	5.32	2.31	0.13	0.35	0.20	0.11	1.51	0.90	0.87	7.29	0.12	3.86	19.40		11.00	11.30	2.78
Na_2O	2.99	4.98	2.70	5.30	5.11	7.07	5.40	4.66	3.51	6.86	7.19	4.91	6.39	2.94	0.32		2.29	2.88	3.60
K_2O	0.83	4.16	0.77	2.46	5.98	5.16	0.83	6.92	1.45	5.38	5.63	1.46	1.13	0.64	0.07		0.82	1.52	0.53
Fe_2O_3	12.30	9.64	14.60	10.80	1.16	6.66	4.56	0.94	5.12	6.77	6.38	12.60	0.63	12.80	0.99		11.40	12.80	8.46
MnO	0.18	0.35	0.21	0.25	0.03	0.25	0.10	0.03	0.12	0.38	0.35	0.21	0.02	0.21	0.21		0.18	0.19	0.17
TiO_2	2.00	0.44	3.31	1.71	0.14	0.64	0.85	0.17	0.52	0.87	0.63	2.30	0.06	1.13	0.07		2.20	2.57	0.60
P_2O_5	0.29	0.06	1.13	0.67	0.05	0.12	0.29	0.07	0.13	0.28	0.16	0.52	0.05	0.31	0.08		0.40	0.64	0.33
H_2O	1.68	3.69	1.88	0.14	0.22	0.66	0.63	0.56	0.15	3.88	4.05	1.16	0.57	0.59	44.90		1.92	1.36	0.43
Total	100.24	98.86	99.62	99.36	98.74	99.21	99.76	98.86	99.37	99.07	98.78	99.95	99.38	99.77	99.33		100.21	99.36	99.72
Normative																			
Q	–	26.80	–	–	10.70	2.03	30.80	9.32	37.40	–	–	–	32.20	3.50	–		–	–	18.10
C	–	–	–	–	0.74	–	0.89	1.23	2.70	–	–	–	2.26						
Or	4.91	24.60	4.55	14.50	35.30	30.50	4.91	40.90	8.57	31.80	33.30	8.63	6.68	3.78	–		4.85	8.98	3.13
Ab	17.40	24.30	22.80	44.80	43.20	51.00	45.70	39.40	29.70	35.30	28.70	9.18	54.10	24.90	–		15.50	8.11	30.50
An	22.60	–	26.00	11.80	6.22	–	8.52	5.50	8.87	1.61	0.48	13.80	2.20	30.50	0.79		25.00	16.70	22.40
Ne	4.27	–	–	–	–	–	–	–	–	12.30	17.40	17.50	–	–	1.47		2.12	8.81	
Kp	–	–	–	–	–	–	–	–	–	–	–	–	–	–	73.00				
Di	27.20	2.16	17.40	9.02	–	3.66	–	–	–	4.06	6.85	28.40	–	13.00	–		22.80	25.00	8.98
Hy	–	11.20	2.93	7.78	1.38	6.72	4.14	1.05	8.58	–	–	–	0.90	15.30	–		–	–	10.80
Ol	12.60	–	9.03	1.92	–	–	–	–	–	4.90	3.72	10.50	–	–	34.80		18.20	18.70	
Cs	–	–	–	–	–	–	–	–	–	–	–	–	–	–	44.00				
Mt	4.18	–	4.96	3.71	0.40	–	1.56	0.33	1.76	2.41	2.27	4.29	0.22	4.36	0.41		3.88	4.35	2.89
Il	3.80	0.84	6.29	3.25	0.27	1.22	1.61	0.32	0.99	1.65	1.20	4.37	0.11	2.15	0.13		4.18	4.88	1.14
AP	0.67	0.14	2.62	1.55	0.12	0.28	0.67	0.16	0.30	0.65	0.37	1.20	0.12	0.72	0.19		0.93	1.48	0.76

Table 3
Compressional wave velocities in km/s as a function of pressure

Sample	Orientation	Density (g/cm^3)	P (MPa)							
			20	60	100	200	400	600	800	1000
K-2a	A	2.956	6.711	6.748	6.765	6.779	6.785	6.788	6.790	6.792
	B	2.955	6.675	6.710	6.725	6.738	6.744	6.748	6.750	6.752
	C	2.956	6.690	6.724	6.739	6.751	6.756	6.758	6.760	6.761
	Mean	2.956	6.692	6.728	6.744	6.756	6.762	6.765	6.767	6.769
K-3	A	2.935	6.477	6.541	6.565	6.581	6.584	6.586	6.587	6.587
	B	2.941	6.495	6.526	6.542	6.557	6.560	6.560	6.561	6.561
	C	2.929	6.416	6.448	6.462	6.471	6.472	6.472	6.471	6.471
	Mean	2.935	6.463	6.505	6.524	6.537	6.539	6.540	6.540	6.540
K-5	A	2.261	3.957	4.290	4.457	4.683	4.902	5.031	5.123	5.197
	B	2.264	4.194	4.623	4.790	4.948	5.077	5.153	5.208	5.252
	C	2.266	4.337	4.605	4.736	4.897	5.032	5.107	5.162	5.204
	Mean	2.264	4.163	4.506	4.661	4.843	5.004	5.097	5.164	5.218
K-6	A	2.751	5.396	5.510	5.561	5.631	5.700	5.741	5.771	5.793
	B	2.813	5.412	5.557	5.613	5.670	5.720	5.749	5.770	5.786
	C	2.761	5.421	5.546	5.614	5.723	5.850	5.928	5.980	6.017
	Mean	2.775	5.410	5.538	5.596	5.675	5.757	5.806	5.840	5.865
K-7	A	2.670	4.428	4.661	4.781	4.953	5.117	5.205	5.265	5.311
	B	2.684	5.023	5.139	5.201	5.294	5.396	5.453	5.490	5.516
	C	2.676	4.844	5.003	5.085	5.200	5.308	5.365	5.404	5.434
	Mean	2.677	4.765	4.935	5.023	5.149	5.274	5.341	5.387	5.421
K-8	A	2.616	4.820	5.521	5.846	6.136	6.284	6.355	6.406	6.446
	B	2.610	5.007	5.655	5.919	6.134	6.259	6.328	6.377	6.415
	C	2.612	5.441	5.920	6.130	6.303	6.378	6.428	6.458	6.480
	Mean	2.613	5.090	5.699	5.965	6.192	6.310	6.371	6.414	6.448
K-10	A	1.306	1.686	2.189	2.372	2.500	2.572	2.613	2.642	2.666
	B	1.373	1.538	1.898	2.049	2.169	2.233	2.267	2.291	2.310
	C	1.340	1.690	2.055	2.210	2.336	2.401	2.435	2.460	2.479
	Mean	1.340	1.638	2.047	2.210	2.335	2.402	2.438	2.464	2.485
K-14	A	2.679	5.799	5.945	6.012	6.097	6.176	6.222	6.255	6.281
	B	2.665	5.774	5.912	5.978	6.067	6.153	6.203	6.239	6.266
	C	2.686	5.738	5.907	5.981	6.073	6.160	6.211	6.248	6.277
	Mean	2.677	5.771	5.921	5.991	6.079	6.164	6.213	6.248	6.275
K-15	A	2.575	5.346	5.691	5.839	5.984	6.091	6.152	6.196	6.230
	B	2.573	5.368	5.771	5.943	6.116	6.249	6.326	6.382	6.425
	C	2.563	5.143	5.570	5.758	5.924	6.019	6.069	6.105	6.133
	Mean	2.570	5.286	5.678	5.847	6.008	6.120	6.183	6.228	6.263
K-16	A	2.734	5.620	5.869	5.990	6.123	6.218	6.268	6.303	6.331
	B	2.751	5.872	6.062	6.169	6.326	6.466	6.531	6.571	6.600
	C	2.745	5.809	6.049	6.173	6.317	6.417	6.465	6.499	6.526
	Mean	2.743	5.768	5.994	6.112	6.256	6.367	6.422	6.458	6.486
K-17	A	2.511	5.478	5.546	5.584	5.629	5.653	5.661	5.666	5.670
	B	2.518	5.513	5.551	5.572	5.593	5.600	5.602	5.603	5.603
	C	2.525	5.667	5.705	5.719	5.726	5.729	5.731	5.732	5.732
	Mean	2.518	5.553	5.601	5.626	5.650	5.661	5.665	5.667	5.669
K-17a	A	2.557	5.861	5.968	5.993	6.004	6.011	6.015	6.017	6.019
	B	2.561	5.857	5.888	5.901	5.910	5.913	5.914	5.915	5.916
	C	2.556	5.752	5.836	5.857	5.863	5.862	5.861	5.861	5.860
	Mean	2.558	5.824	5.898	5.917	5.926	5.929	5.930	5.931	5.932
K-17b	A	2.976	6.528	6.621	6.647	6.658	6.661	6.662	6.664	6.664
	B	2.966	6.501	6.575	6.616	6.657	6.669	6.670	6.670	6.670
	Mean	2.971	6.515	6.599	6.632	6.658	6.665	6.667	6.667	6.668

et al. (1986) (Fig. 3). For brevity, we refer to the Kenya volcanic rock samples as basalts and phonolites.

Compressional-wave velocities, summarized in Table 3, were measured under hydrostatic confining pressures to 1000 MPa (10 kbar) using a pulse transmission technique similar to that described by Christensen (1985) and Christensen and Wepfer (1989). The samples used for the measurements were cut in the form of right circular cylinders 2.54 cm in diameter and 3–5 cm in length. To study anisotropy, velocities were measured in three core samples taken from each rock in three mutually perpendicular directions. Densities (Table 3) were calculated from the dimensions and weights of the rock cylinders. Pressure-related changes in sample dimensions were considered in calculating velocities.

Room-temperature laboratory measurements have been corrected for high and low geotherms corresponding to the estimated thermal gradients within the rift and on the flanks, respectively. Estimated rift and flank geotherms of 28°C/km and 15°C/km are based on sparse heat flow measurements in Kenya (Morgan, 1983) and on comparisons with estimated geotherms for similar geologic settings (e.g., Lachenbruch and Sass, 1978). We have used an average temperature correction of -0.5×10^{-3} km s^{-1} $°C^{-1}$ based on laboratory results of Kern (1978) and Christensen (1979). The temperature corrections applied for comparisons with seismic velocities within the rift are significant, and amount to velocity reductions (from room-temperature measurements) of approximately 0.14 km/s, 0.28 km/s, and 0.42 km/s at 10 km, 20 km, and 30 km, respectively. Temperature corrections for the low geotherm are about one-half these quantities.

5. Discussion

Complete room-temperature velocity–pressure curves for all Kenya rock samples are shown in Fig. 4A. Temperature-corrected velocities corresponding to the high geotherm are shown in Fig.

Table 3 (continued)

Sample	Orientation	Density (g/cm^3)	P (MPa)							
			20	60	100	200	400	600	800	1000
K-19	A	2.965	5.876	6.081	6.194	6.334	6.424	6.462	6.487	6.506
	B	2.958	6.120	6.354	6.466	6.604	6.726	6.795	6.845	6.883
	C	2.954	5.669	5.987	6.114	6.249	6.372	6.445	6.497	6.538
	Mean	2.959	5.889	6.141	6.256	6.396	6.508	6.568	6.610	6.643
K-20	A	2.390	4.750	4.828	4.867	4.917	5.956	4.977	4.991	5.002
	B	2.396	4.798	4.867	4.901	4.941	4.975	4.994	5.007	5.017
	C	2.365	4.785	4.853	4.888	4.946	5.009	5.047	5.074	5.095
	Mean	2.384	4.778	4.849	4.885	4.935	5.313	5.006	5.024	5.038
K-21	A	2.971	6.468	6.521	6.536	6.558	6.596	6.627	6.651	6.671
	B	2.954	6.226	6.338	6.387	6.442	6.492	6.521	6.542	6.558
	C	2.954	6.183	6.320	6.385	6.471	6.556	6.606	6.642	6.670
	Mean	2.960	6.293	6.394	6.437	6.491	6.548	6.585	6.612	6.633
K-21a	A	3.020	6.243	6.282	6.306	6.350	6.411	6.454	6.486	6.509
	B	3.018	6.172	6.217	6.244	6.289	6.348	6.386	6.412	6.431
	C	3.019	6.229	6.268	6.284	6.326	6.390	6.431	6.460	6.483
	Mean	3.019	6.215	6.256	6.278	6.322	6.384	6.424	6.453	6.475
K-30	A	2.788	5.307	5.657	5.827	6.024	6.181	6.269	6.332	6.381
	B	2.795	5.720	6.058	6.236	6.434	6.553	6.606	6.642	6.671
	C	2.829	6.113	6.312	6.417	6.562	6.689	6.753	6.797	6.830
	Mean	2.804	5.714	6.009	6.160	6.340	6.475	6.543	6.591	6.628

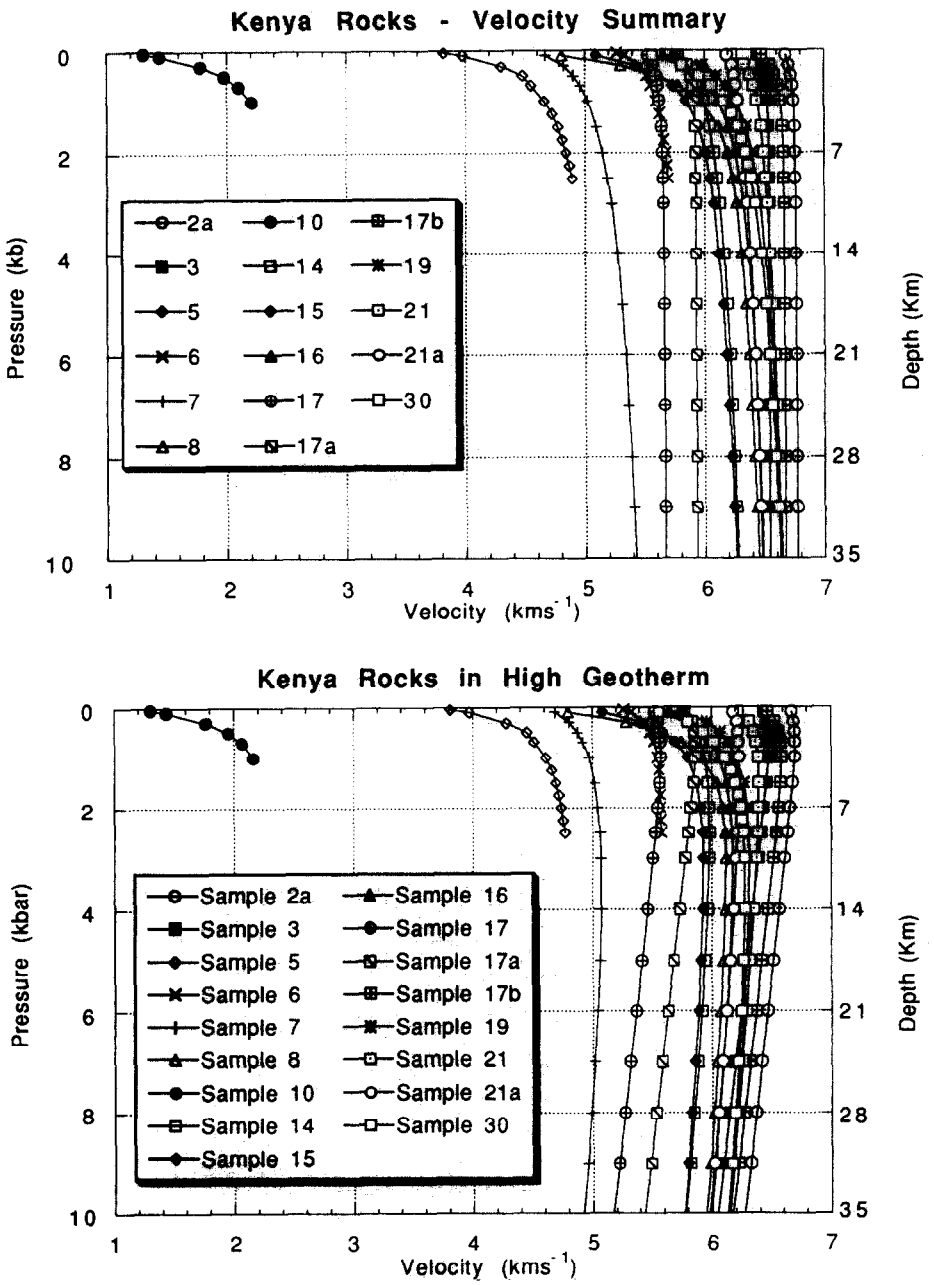

Fig. 4. (A) Summary of all laboratory seismic velocity measurements made on seventeen Kenya rock samples. Sample numbers refer to Fig. 1 (location map), Table 1 (mineralogy), Table 2 (chemical composition), and Table 3 (seismic velocities). (B) Kenya rock samples with high geotherm temperature correction applied (see text). The observed negative velocity gradients are not uncommon for rock samples, and are due to the dominant effect of temperature in reducing seismic velocity (Christensen, 1979); the effect of increased pressure alone is visible in (A). The highest velocities are for basalts and phonolites. Gneissic rocks show uniformly lower velocities, and volcanic tuffs are lowest in velocity.

4B. The correction is particularly significant in the middle and lower crust, where temperatures are higher.

Referring to Fig. 4A, velocities of 5.4 km/s to 6.8 km/s are measured at 400 MPa (4 kbar, equivalent to 14 km depth). High-density volcanic rocks have the highest velocities (6.6–6.8 km/s at 400 MPa), and low-density tuffs show the lowest velocities (2.2 km/s at 100 MPa). Reliable correlations between seismic velocity and mineralogy of the volcanic rocks are difficult to determine because of the fine grain size and alteration products common to these rocks. However, samples with abundant pyroxene phenocrysts (K-2 and K-17b) tend to have higher velocities than samples with plagioclase phenocrysts (K-21a; Table 1).

The highest-velocity gneissic rocks (K-19 and K-30) contain a higher percentage of hornblende, whereas the lower-velocity rocks are granitic gneisses (K-14 and K-15) with high percentages of potash feldspar and quartz, and are garnet-free (Table 1). Seismic anisotropy in these metamorphic rocks at 400 MPa ranges between 0.5% and 5.5%, and averages about 3%. This average amount of velocity anisotropy is equal to the estimated measurement error of deep crustal velocities (e.g., Mooney, 1989), and indicates that velocity anisotropy is a significant factor in interpreting deep crustal velocities and composition. The low densities and seismic velocities of the volcanic tuffs originate from the high porosities and alteration products within these rocks.

These laboratory measurements of seismic velocities provide significant constraints on the likely composition of the crustal layers defined in the KRISP-90 seismic refraction profiles. We present comparisons of field and laboratory measurements for three separate areas: the east flank (recording line E, Fig. 1) of the rift (Fig. 5), the southern rift (Fig. 6), and the northern rift (Fig. 7). The northern and southern rifts are treated separately because the crustal structure is significantly different (Fig. 2). Temperature corrections for a low geotherm, as discussed above, are used for the flank profile, and corrections for a high geotherm are used within the rift.

5.1. Supracrustal rocks (tuffs, basalts and phonolites)

Seismic velocities of supracrustal volcanic rocks within the rift range from 1.9 to 5.15 km/s, and extend to depths as great as 6 km (corresponding to about 175 MPa (1.75 kbar); Fig. 2). The lowest field velocities (2.0–2.2 km/s) are consistent with those measured for sample K-10, an ash-fall tuff with a density of 1.34 g/cm. However, the basalts, phonolites and other volcanic rocks, which clearly constitute a significant portion of the supracrustal geologic section, have laboratory-measured velocities higher than the 3.1–5.15 km/s velocities recorded within the rift. This discrepancy between laboratory and field measurements is most likely due to extensive fracturing, jointing, and rubble zones in the basalts common to volcanic flows elsewhere. Abundant tuffs interlayered with basalt flows are also consistent with the field measurements. High pore pressures in these porous rocks may also be an important factor in lowering velocities (Spencer and Nur, 1976; Christensen, 1989).

5.2. Crystalline basement (upper crust)

Upper crustal seismic velocities range from 6.0 to 6.3 km/s on the three KRISP-90 profiles (Fig. 2). The east flank profile and the western and eastern portions of the cross-profile were recorded outside of the rift where the basement metamorphic complex is exposed (Fig. 1). A comparison of the upper crustal velocities with the Kenya metamorphic rock samples shows excellent agreement (Figs. 5A, 6A, and 7A). While it is perhaps not unexpected that the metamorphic rocks would agree with the upper crustal velocities for the flank profiles (Fig. 5A), the agreement with the southern and northern rift profiles (Fig. 6A and 7A) strongly suggests that these gneissic rocks are also the dominant rock type beneath the rift. The basalts and phonolites measured in this study show velocities uniformly in excess of 6.2 km/s. Since the intrusive equivalents of these volcanics (gabbro and syenite) have higher velocities, it appears that these rocks are

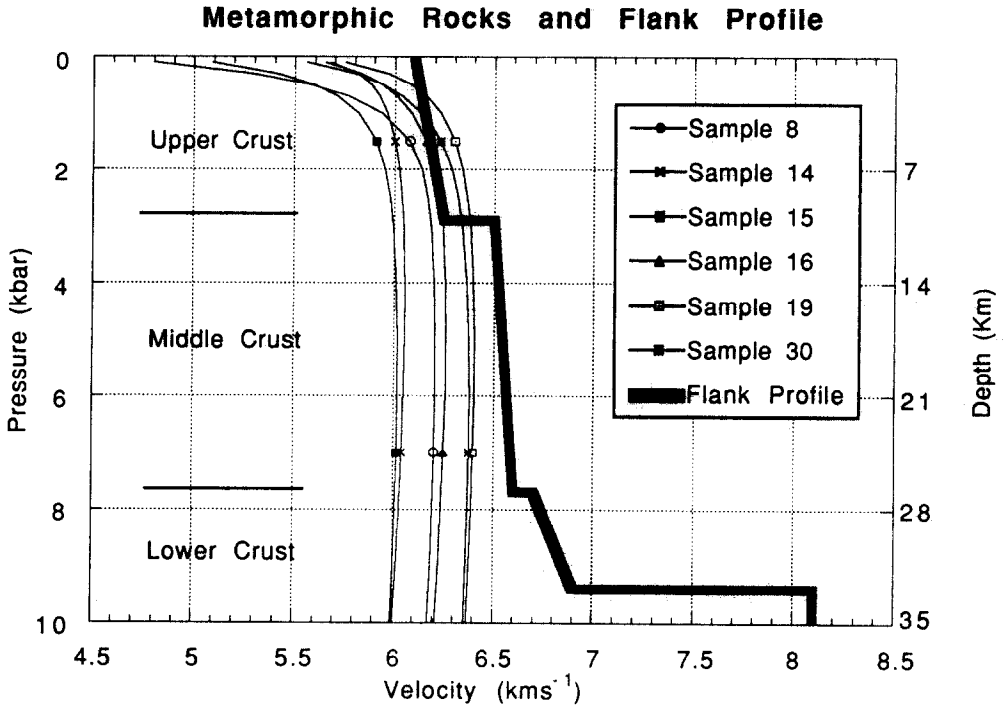
Metamorphic Rocks and Flank Profile
Upper Crust
Middle Crust
Lower Crust
Sample 8
Sample 14
Sample 15
Sample 16
Sample 19
Sample 30
Flank Profile
Pressure (kbar)
Depth (Km)
Velocity (kms-1)
0
2
4
6
8
10
7
14
21
28
35
4.5
5
5.5
6
6.5
7
7.5
8
8.5

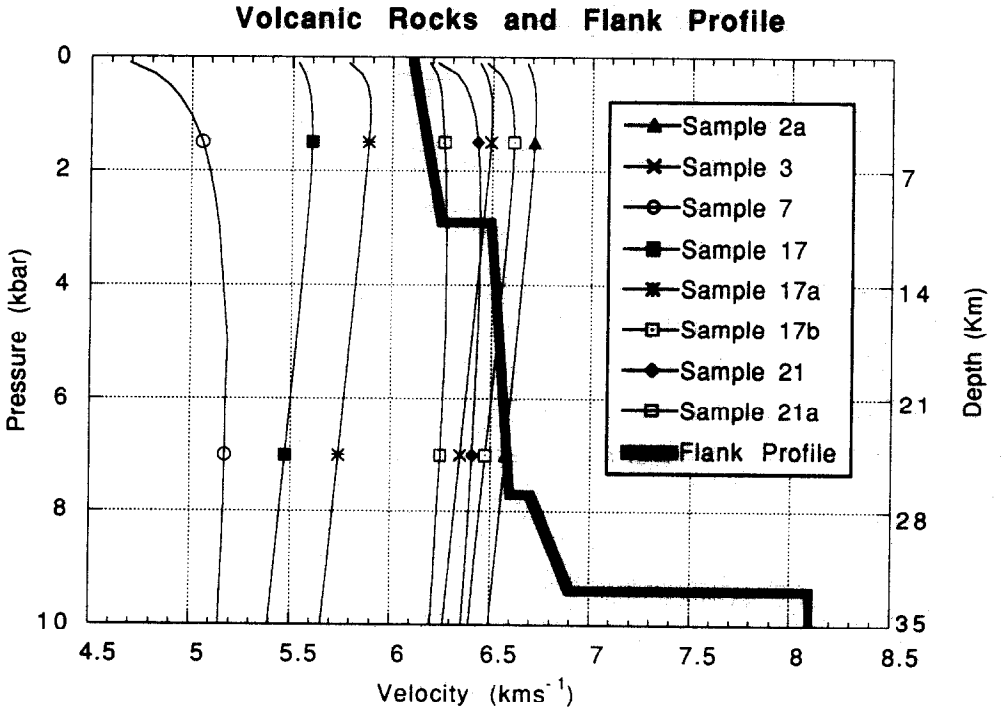
Volcanic Rocks and Flank Profile
Sample 2a
Sample 3
Sample 7
Sample 17
Sample 17a
Sample 17b
Sample 21
Sample 21a
Flank Profile
Pressure (kbar)
Depth (Km)
Velocity (kms-1)
0
2
4
6
8
10
7
14
21
28
35
4.5
5
5.5
6
6.5
7
7.5
8
8.5

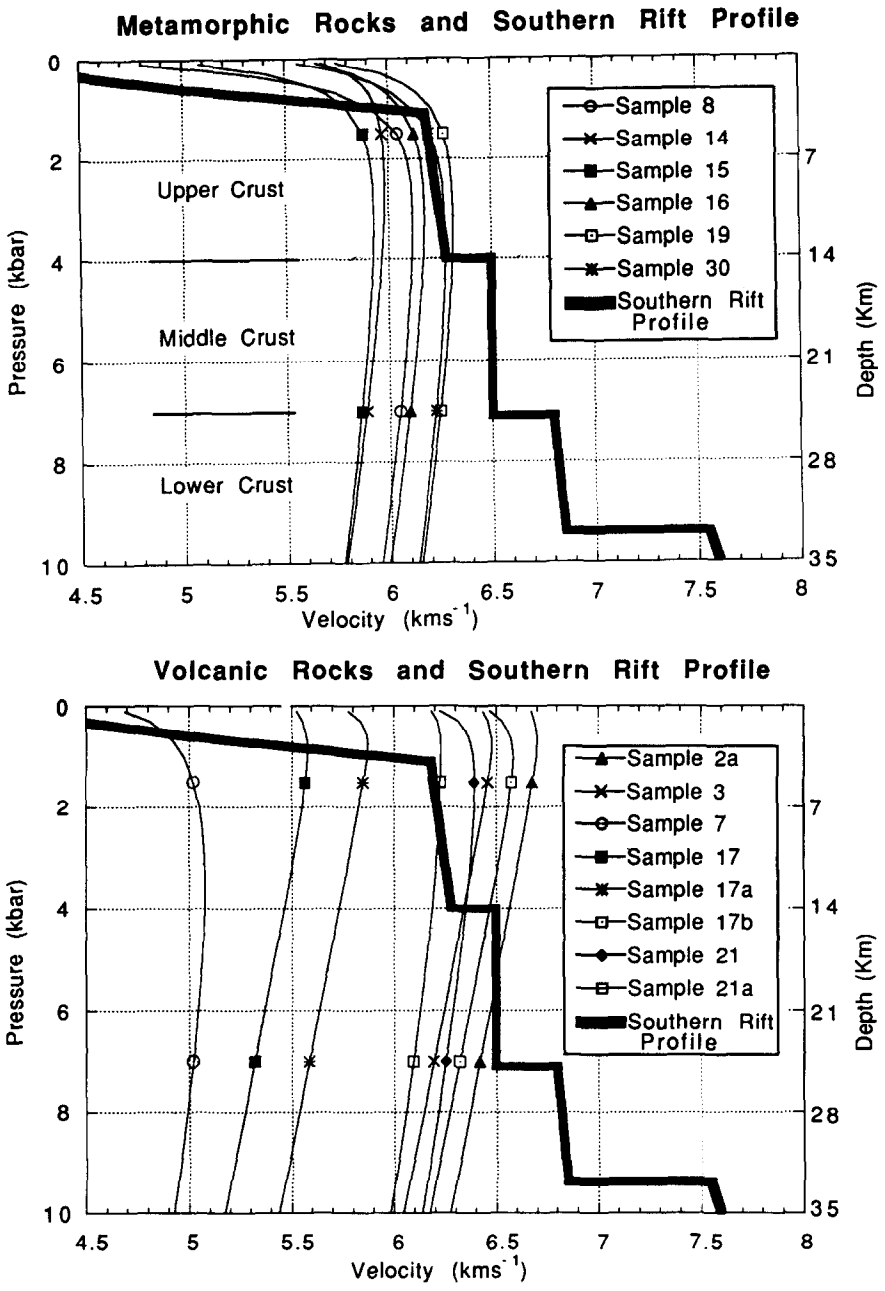

Fig. 6. Comparison of the average velocity/depth structure beneath the southern portion of the axial rift profile (Fig. 2) with (A) Kenya metamorphic rocks and (B) volcanic rocks. Sample numbers are keyed to Fig. 1 and Tables 1–3. The two seismic discontinuities in the crust at 14 km and 25 km define the upper, middle and lower crust. The upper mantle velocity is 7.6 km/s.

Fig. 5. Comparison of the average velocity–depth structure beneath the east flank profile (Fig. 2) with (A) Kenya metamorphic rocks and (B) volcanic rocks. Sample numbers are keyed to Fig. 1 and Tables 1–3. The two seismic discontinuities in the crust at 10 km and 26 km define the upper, middle and lower crust. The upper-mantle velocity is 8.1 km/s. The estimated error in crustal velocities is 3%, or ± 0.2 km/s.

not abundant constituents of the upper crust of the rift.

It is apparent from the comparison of field and laboratory velocities (Figs. 5–7) that the rock samples show negative velocity–depth gradients (due to the effects of temperature), whereas the

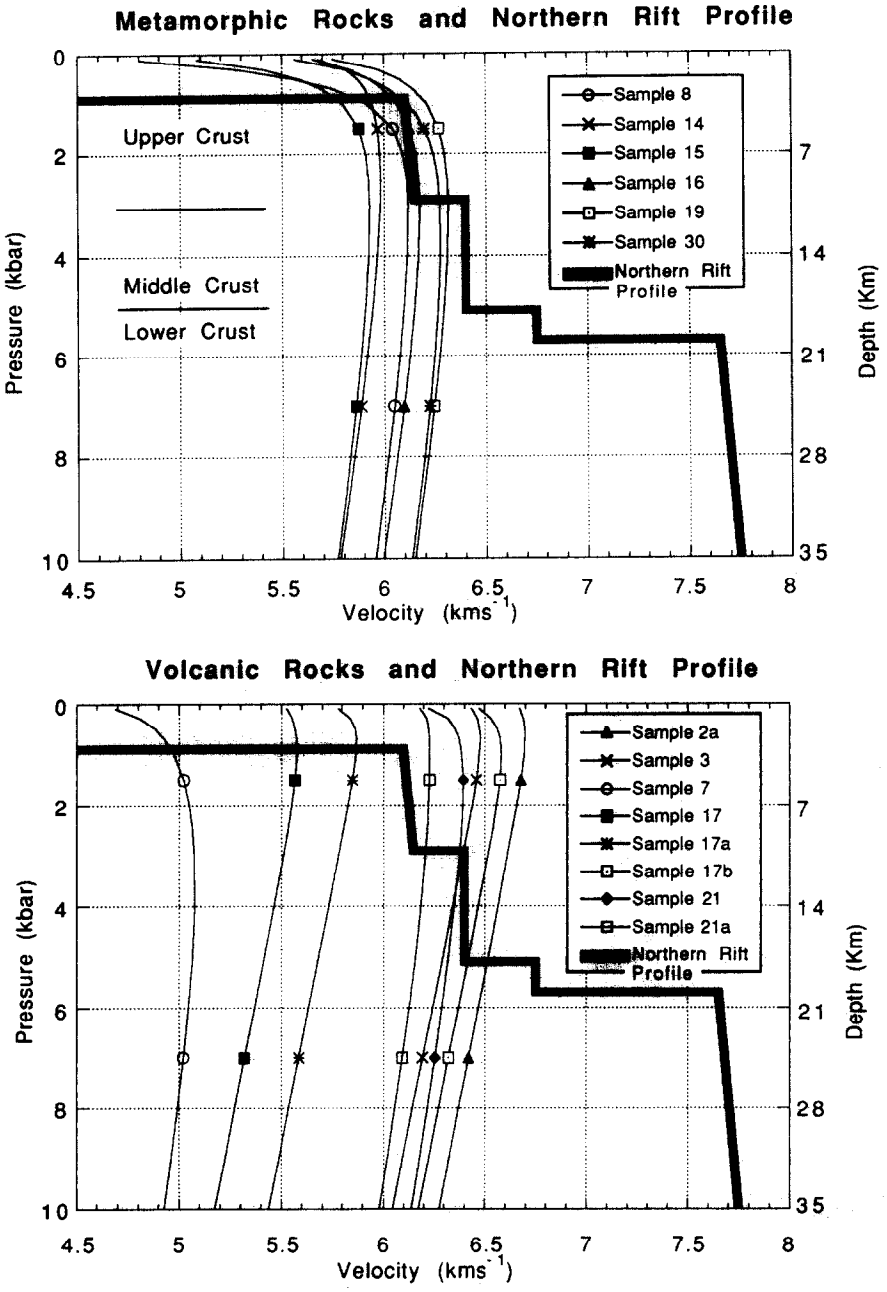

Fig. 7. Comparison of the average velocity/depth structure beneath the northern portion of the axial rift profile (Fig. 2) with (A) Kenya metamorphic rocks and (B) volcanic rocks. Sample numbers are keyed to Tables 1 and 2. The two seismic discontinuities in the crust at 10 km and 18 km define the upper, middle and lower crust. The lower crustal layer is only 2–3 km thick. The upper mantle, at 20–21 km depth, has a velocity of 7.6–7.7 km/s.

reported crustal structure shows a positive or zero gradient. The most plausible explanation is that crustal composition progressively changes with depth towards increasingly mafic rocks. This explanation is consistent with exposed deep crustal sections (e.g., Percival and Card, 1985; Percival et al., 1992).

5.3. Middle crust

A velocity of approximately 6.5 km/s is measured at a depth of 10–15 km beneath all three seismic refraction profiles. Inferring crustal composition at these depths is less reliable than for the upper crust, where crystalline basement rocks are exposed, and admits multiple possibilities. Therefore we focus our discussion to two end-member hypotheses that can be constrained by our data: a middle crust consisting either of intermediate-composition gneissic rocks (e.g., dioritic gneiss, sample K-19) or of the intrusive equivalents of basalts and phonolites (e.g., samples K-3 and K-21).

Considering first the flank profile (Fig. 5), the metamorphic rocks show lower velocities than the middle crust, although the intermediate composition gneisses (samples K-19 and K-30) are only 0.2–0.3 km/s too low. This suggests that somewhat more mafic, perhaps higher-grade metamorphic rocks are reasonable candidate compositions for the middle crust of the rift-flanking area. Several of the volcanic rocks have higher seismic velocities than the metamorphic rocks and provide excellent agreement with the measured middle-crustal velocities. However, it should be noted that coarser-grained intrusive equivalents to these extrusive rocks would have still higher seismic velocities (6.7–7.0 km/s) at these depths (e.g., Birch, 1960). On balance, we favor gneisses of intermediate composition for the middle crust of the rift flank. Such an intermediate crustal composition is consistent with tonalitic gneisses in exposed crustal sections of Archean and Proterozoic rocks (e.g., Percival and Card, 1985; Percival et al., 1992).

A comparison of the laboratory measurements with the seismic velocities measured in the middle crust beneath the southern and northern rift suggests that metamorphic rocks of higher metamorphic grade than those exposed at the surface, or mafic intrusive rocks are possible compositions of the crust. A mixture of these rocks (i.e., gneisses intruded by mafic dikes) is also a reasonable composition.

5.4. Lower crust

The lower crust beneath the Kenya rift and its flanking areas has seismic velocities of 6.7–7.0 km/s and varies laterally in thickness (Fig. 2). This layer is 9 km thick beneath the southern rift, and thins to 2–3 km beneath the northern rift. The layer is laterally continuous across the rift, and maintains an average thickness of about 8–9 km on the cross-profile (Fig. 2). On the flank profile, the lower crustal layer is interpreted to be about 8 km thick beneath the middle of the profile, and thins to the northwest and southeast.

The lower crustal velocities of 6.7–7.0 km/s are higher than any of the velocities measured in the felsic to intermediate gneisses collected along the rift flanks. Thus, lower crustal analogues are not exposed in the region. Based on the Proterozoic geology of Kenya, and on published velocity comparisons, amphibolite to granulite facies mafic rocks are probably constituents in the lower crust on the flanks of the rift (Christensen and Fountain, 1975; Holbrook et al., 1992; Mosley, 1993).

The temperature-corrected seismic velocities of the metamorphic and volcanic rocks are about 1.0 km/s lower than the measured lower crustal velocities beneath the southern rift (Fig. 6), which indicates that significantly denser, more mafic rocks are found at these depths. The lower crustal velocities of the southern rift are intermediate between the seismic velocities of the middle crust and the upper mantle. Given the high heat flow and abundant volcanics within the rift, we concur with Baker et al. (1972) that the lower crust largely consists of a mafic residuum accreted to the base of the crust during the differentiation of an upper mantle melt.

The lower crustal layer beneath the northern rift is only 0.2 km/s higher in velocity than one of the Kenya volcanic rock samples (Fig. 7B). This suggests that a significant basal crustal residuum

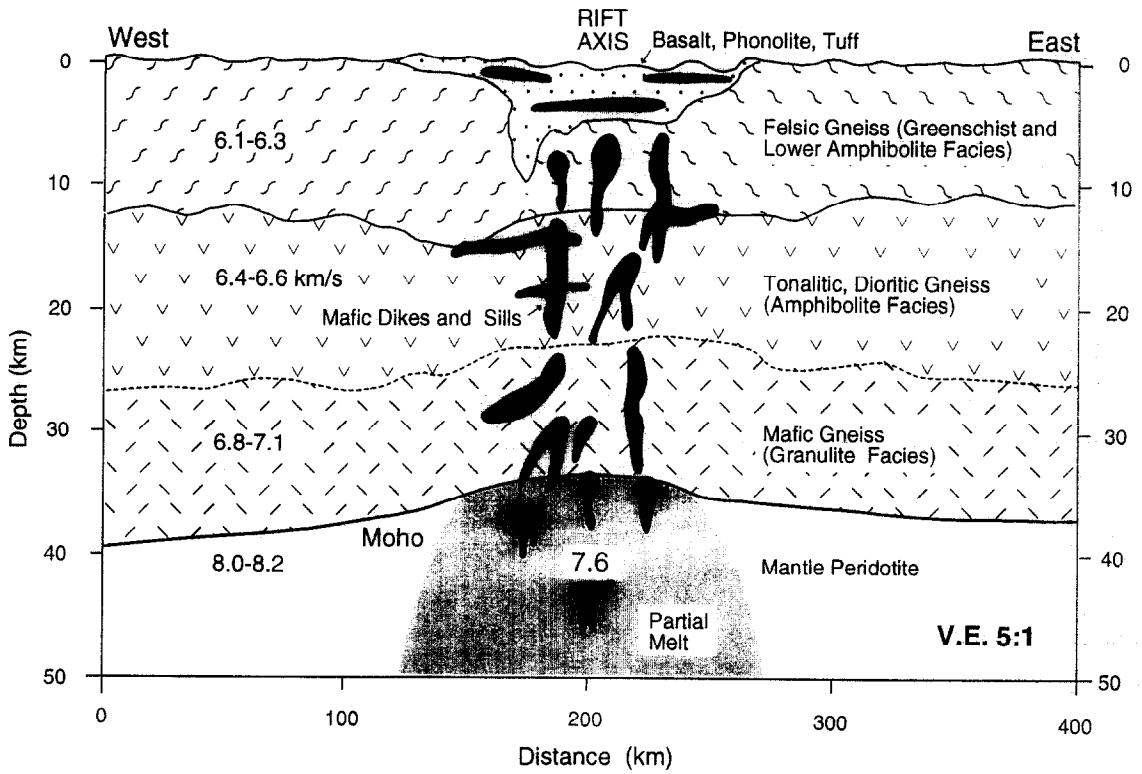

Fig. 8. Composition of the crust beneath the Kenya rift at the Equator based on a comparison of crustal seismic velocity structure (Maguire et al., 1994; Braile et al., 1994) with laboratory measurements of Kenyan rock samples. The crust is comprised of three primary layers whose composition increases with depth from felsic to mafic, and in metamorphic grade from greenschist to granulite facies. The crust beneath the rift axis probably contains abundant mafic intrusives. An upper mantle partial melt is indicated by the anomalously low upper mantle seismic velocity (7.5–7.7 km/s).

is not present in the northern rift beneath Lake Turkana, and that the extrusive rocks there are mainly produced by differentiation in the upper mantle, which occurs at a depth of only 22 km in this portion of the rift. Referring to Fig. 7A, it is apparent that metamorphic rocks may constitute the bulk of the crust, and therefore, the basaltic extrusives may pass through the crustal column in the northern rift with only minimal mixing with crustal rocks.

6. Conclusions

A comparison of the results of the KRISP-90 seismic-refraction investigation with temperature-corrected laboratory measurements of rock velocities shows that reasonable inferences of crustal composition can be made (Fig. 8). On the flanks of the rift, the upper and middle crust appear to be comprised largely of Precambrian greenschist to amphibolite facies felsic-to-intermediate composition metamorphic rocks. The lower crust on the flanks of the rift may consist of granulite facies mafic rocks. The upper and middle crustal layers appear to be continuous from the eastern rift flank to the western flank, but these layers are most likely intruded by mafic dikes and sills beneath the rift. The lower crust beneath the rift probably consists of a mix of high-grade metamorphic rocks, mafic intrusions, and an igneous mafic residuum accreted to the base of the crust during differentiation of a melt derived from the upper mantle.

Acknowledgements

Discussions with members of the KRISP-90 Working Group, particularly J. Mechie, G.R.

Keller, and C. Prodehl, significantly improved the ideas presented here. Permission to collect and remove samples from Kenya was granted by the Government of Kenya, and is gratefully acknowledged. Reviews by B. Beaudoin, H. Kern, C. Prodehl, S.B. Smithson improved the text; D. Evans and R. Mandel assisted in the preparations of the figures.

References

Baker, B.H., Mohr, P.A. and Williams, L.A.J., 1972. Geology of the eastern rift system of Africa. Geol. Soc. Am., Spec. Pap., 136 pp.

Birch, F., 1960. Compressional wave velocities in rocks down to 10 kbar, Part 1. J. Geophys. Res., 65: 1083–1102.

Braile, L.W., Wang, B., Daudt, C.R., Keller, G.R. and Patel, J.P., 1994. Modelling the 2-D velocity structure across the Kenya rift. In: C. Prodehl, G.R. Keller and M.A. Khan (Editors), Crustal and Upper Mantle Structure of the Kenya Rift. Tectonophysics, 236: 251–269.

Christensen, N.I., 1979. Compressional wave velocities in rocks at high temperatures and pressures, critical thermal gradients and crustal low velocity zones. J. Geophys. Res., 84: 6849–6857.

Christensen, N.I., 1985. Measurements of dynamic properties of rocks at elevated pressures and temperatures. In: H.J. Pincus and E.R. Hoskins (Editors), Measurements of Rock Properties at Elevated Pressures and Temperatures. American Society of Testing and Materials ASTM STP869, Philadelphia, Penn., pp. 93–107.

Christensen, N.I., 1989. Pore pressure, seismic velocities, and crustal structure. In: L. Pakiser and W.D. Mooney (Editors), Geophysical Framework of the Continental United States. Geol. Soc. Am. Mem., 172: 783–798.

Christensen, N.I. and Fountain, D.M., 1975. Constitution of the lower continental crust based on experimental studies of seismic velocities in granulite. Geol. Soc. Am. Bull., pp. 227–236.

Christensen, N.I. and Wepfer, W.W., 1989. Laboratory techniques for determining seismic velocities and attenuations, with application to the continental lithosphere. In: L. Pakiser and W.D. Mooney (Editors), Geophysical Framework of the Continental United States. Geol. Soc. Am. Mem., 172: 91–102.

Gajewski, D., Schulte, A., Riaroh, D. and Thybo, H., 1994. Deep seismic sounding in the Turkana depression, northern Kenya rift. In: C. Prodehl, G.R. Keller and M.A. Khan (Editors), Crustal and Upper Mantle Structure of the Kenya Rift. Tectonophysics, 236: 165–178.

Holbrook, W.S., Mooney, W.D. and Christensen, N.I., 1992. The seismic velocity structure of the deep continental crust. In: D.M. Fountain, R. Arculus and R. Kay (Editors), Continental Lower Crust. Elsevier, Amsterdam, pp. 1–43.

Keller, G.R., Prodehl, C., Mechie, J., Fuchs, K., Khan, M.A., Maguire, P.K.H., Mooney, W.D., Achauer, U., Davis, P.M., Meyer, R.P., Braile, L.W., Nyambok, I.O. and Thompson, G.A., 1994. The East African rift system in the light of KRISP 90. In: C. Prodehl, G.R. Keller and M.A. Khan (Editors), Crustal and Upper Mantle Structure of the Kenya Rift. Tectonophysics, 236: 465–483.

Kern, H., 1978. The effect of high temperature and high confining pressure on compressional wave velocities in quartz-bearing and quartz-free igneous and metamorphic rocks. Tectonophysics, 44: 185–203.

KRISP Working Party, 1991. Large-scale variations in lithospheric structure along and across the Kenya Rift. Nature, 354: 223–227.

Lachenbruch, A.H. and Sass, J.H., 1978. Models of an extending lithosphere and heat flow in the Basin and Range province. In: R.B. Smith and G.P. Eaton (Editors), Cenozoic Tectonics and Regional Geophysics of the Western Cordillera. Geol. Soc. Am. Mem., 152: 209–250.

LeBas, M.J., LeMaitre, R.W., Streckeisen, A. and Zanetin, B., 1986. A chemical classification of volcanic rocks based on the total alkali-silica diagram. J. Petrol. 27: 745–750.

Maguire, P.K.H., Swain, C.J., Masotti, R. and Khan, M.A., 1994. A crustal and uppermost mantle cross-sectional model of the Kenya Rift derived from seismic and gravity data. In: C. Prodehl, G.R. Keller and M.A Khan (Editors), Crustal and Upper Mantle Structure of the Kenya Rift. Tectonophysics, 236: 217–249.

Mechie, J., Keller, G.R., Prodehl, C., Gaciri, S., Braile, L.W., Mooney, W.D., Gajewski, D. and K.-J. Sandmeier, 1994. Crustal structure beneath the Kenya Rift from axial profile data. In: C. Prodehl, G.R. Keller and M.A. Khan (Editors), Crustal and Upper Mantle Structure of the Kenya Rift. Tectonophysics, 236: 179–199.

Mooney, W.D., 1989. Seismic methods for determining earthquake source parameters and lithospheric structure. In: L. Pakiser and W.D. Mooney (Editors), Geophysical Framework of the Continental United States. Geol. Soc. Am. Mem., 172: 11–34.

Morgan, P., 1983. Constraints on rift thermal processes from heat flow and uplift. Tectonophysics, 94: 277–298.

Morley, C.K., Westcott, W.A., Stone, D.M., Harper, R.M., Wigger, S.T. and Karanja, F.M., 1992. Tectonic evolution of the northern Kenya rift. J. Geol. Soc. London, 149: 333–348.

Morley, C.K., 1994. Interaction of deep and shallow processes in the evolution of the Kenya rift. In: C. Prodehl, G.R. Keller and M.A. Khan (Editors), Crustal and Upper Mantle Structure of the Kenya Rift. Tectonophysics, 236: 81–91.

Mosley, P.N., 1993. Geological evolution of the late Proterozoic "Mozambique Belt" of Kenya. Tectonophysics, 221: 223–250.

Percival, J.A. and Card, K.D., 1985. Structure and evolution of Archean crust in central Superior province, Canada. In: L.D. Ayers, P.C. Thurston, K.D. Card and E. Weber (Editors), Evolution of Archean Supracrustal Sequences. Geol. Assoc. Can. Spec. Pap., 28: 179–192.

Percival, J.A., Fountain, D.M. and Salisbury, M.H., 1992. Exposed crustal cross sections as windows on the lower crust. In: D.M. Fountain, R. Arculus and R. Kay (Editors), Continental Lower Crust. Elsevier, Amsterdam, pp. 317–362.

Prodehl, C., Mechie, J., Achauer, U., Keller, G.R., Khan, M.A., Mooney, W.D., Gaciri, S.J. and Obel, J.D., 1994a. The KRISP 90 seismic experiment—a technical review. In: C. Prodehl, G.R. Keller and M.A. Khan (Editors), Crustal and Upper Mantle Structure of the Kenya Rift. Tectonophysics, 236: 33–60.

Prodehl, C., Jacob, B., Thybo, H., Dindi, E. and Stangl, R., 1994b. Crustal structure on the northeastern flank of the Kenya rift. In: C. Prodehl, G.R. Keller and M.A. Khan (Editors), Crustal and Upper Mantle Structure of the Kenya Rift. Tectonophysics, 236: 271–290.

Smith, M., 1994. Stratigraphic and structural constraints on mechanisms of active rifting in the Gregory rift, Kenya. In: C. Prodehl, G.R. Keller and M.A. Khan (Editors), Crustal and Upper Mantle Structure of the Kenya Rift. Tectonophysics, 236: 3–22.

Spencer, J.W. and Nur, A.M., 1976. The effects of pressure, temperature, and pore water on velocities in Westerly granite. J. Geophys. Res., 81: 899–904.

Swain, C.J., Maguire, P.K.H. and Khan, M.A., 1994. Geophysical experiments and models of the Kenya Rift before 1989. In: C. Prodehl, G.R. Keller and M.A. Khan (Editors), Crustal and Upper Mantle Structure of the Kenya Rift. Tectonophysics, 236: 23–32.

Williams, L.A.J., 1972. The Kenya Rift volcanics: a note on volumes and chemical compositions. Tectonophysics, 15: 83–96.